Available online at www.sciencedirect.com
ScienceDirect
Journal of Power Sources 164 (2007) 688–696
JOURNAL OF POWER SOURCES
www.elsevier.com/locate/jpowsour

A three-dimensional mixed-domain PEM fuel cell model with fully-coupled transport phenomena

Hua Meng *

Center for Engineering and Scientific Computation, College of Computer Science, P.O. Box 1455, Zhejiang University, Hangzhou, Zhejiang 310027, PR China

Received 5 September 2006; received in revised form 21 October 2006; accepted 23 October 2006
Available online 4 December 2006

Abstract

A three-dimensional mixed-domain PEM fuel cell model with fully-coupled transport phenomena has been developed in this paper. In this model, after fully justified simplifications, only one set of interfacial boundary conditions is required to connect the water content equation inside the membrane and the equation of the water mass fraction in the other regions. All the other conservation equations are still solved in the single-domain framework. Numerical results indicate that although the fully-coupled transport phenomena produce only minor effects on the overall PEM fuel cell performance, i.e. average current density, they impose significant effects on current distribution, net water transfer coefficient, velocity and density variations, and species distributions. Intricate interactions of the mass transfer across the membrane, electrochemical kinetics, density and velocity variations, and species distributions dictate the detailed cell performances. Therefore, for accurate PEM fuel cell modeling and simulation, the effects of the fully-coupled transport phenomena could not be neglected.

Keywords: PEM fuel cell; Mixed-domain model; Interfacial boundary condition; Fully-coupled transport phenomena; Water content

1. Introduction

Significant progress has been achieved in PEM fuel cell modeling in recent years. The existing multi-dimensional numerical models can generally be classified into two categories, namely the single-domain [1–6] and the multi-domain methods [7–10]. In the single-domain approach, one set of conservation equations is established for the entire computational domain while special numerical treatments are applied to turn on/off a specific equation in specific regions of a PEM fuel cell. This renders a relatively simple method in terms of the mathematical formulation and numerical implementation into general CFD packages. However, an inherent weakness of the single-domain method lies in its inability to directly handle species transport, especially water transport, across the membrane. In order to overcome this deficiency and simultaneously maintain the simplicity, a mixed-domain approach has recently been developed [11]. In this mixed-domain PEM fuel cell model, the conservation equation of the water concentration is solved only in the gas channels, gas diffusion layers (GDL), and catalyst layers on the anode and cathode sides while a conservation equation of the water content is solved in the membrane. These two equations are then connected using a set of internal boundary conditions at the interfaces between the membrane and the two catalyst layers. In addition, a fictitious water concentration treatment [12,13] is used for considering water transport in the membrane phase in the two catalyst layers. All the other conservation equations, including the mass, momentum, species concentrations, proton and electron transport, and energy, remain within the single-domain framework. Numerical studies have shown that this mixed-domain method provides accurate results in terms of not only the cell performances and current distributions but also the water content variations inside the membrane [11].

The mixed-domain model [11] is, however, still incomplete with regards to the interactions of the velocity field and the species transport processes. In other words, the velocity field is still decoupled from the species transport equations in the model. In order to fully integrate the various transport phenomena, the effects of species transport and electrochemical reactions on the mass and momentum conservation equations have to be taken

* Tel.: +86 571 87953166; fax: +86 571 87953167.
E-mail address: menghua@zju.edu.cn.

0378-7753/$ – see front matter © 2006 Elsevier B.V. All rights reserved.
doi:10.1016/j.jpowsour.2006.10.086

Nomenclature

a	water activity or stoichiometry parameter for species component
A	surface area (m^2)
C_p	constant-pressure heat capacity ($J\,kg^{-1}\,K^{-1}$)
D	mass diffusivity ($m^2\,s^{-1}$)
D_λ	water content diffusivity ($mol\,m^{-1}\,s^{-1}$)
F	Faraday constant, 96487C mol^{-1}
i	current density vector ($A\,m^{-2}$)
I_{avg}	average current density ($A\,m^{-2}$)
j	transfer current density ($A\,m^{-3}$)
k	thermal conductivity ($W\,m^{-1}\,K^{-1}$)
m	mass flux ($kg\,m^{-2}\,s^{-1}$)
M	chemical components in electrochemical reactions
n	stoichiometry parameter for electron
n_d	electro-osmotic drag coefficient
N	total number of species components
N_w	net water flux through the membrane ($mol\,m^{-2}\,s^{-1}$)
p	pressure (Pa)
q	interfacial flux ($kg\,m^{-2}\,s^{-1}$)
R_u	universal gas constant ($J\,mol^{-1}\,K^{-1}$)
S	source term
T	temperature (K)
u	velocity ($m\,s^{-1}$)
V	volume (m^3)
W	molecular weight ($kg\,mol^{-1}$)
Y	mass fraction

Greek letters

α	net water transfer coefficient
δ	thickness (m)
ε	porosity
Φ	phase potential (V)
κ	proton conductivity ($S\,m^{-1}$)
λ	water content
μ	chemical potential
ρ	density ($kg\,m^{-1}$)
σ	electronic conductivity ($S\,m^{-1}$)
τ	viscous stress tensor

Subscripts

cl	catalyst layer
e	electrolyte or energy
i	species or interface
m	membrane, mass, or mixture
s	electron
w	water

Superscripts

cl	catalyst layer
eff	effective value
m	membrane

into account properly, meaning that additional source/sink terms have to be included in these equations, especially in the mass conservation equation, as proposed in [2,14,15]. This is a unique feature of the PEM fuel cells, distinct from the other chemically reacting flows, i.e. those in combustion and propulsion systems. This can be attributed to the fact that in PEM fuel cells, where the reactants are consumed is not where the products are produced. In fact, after the HOR reaction on the anode side the protons and electrons could leave the flow-field, get into the other regions, i.e. the membrane and the carbon material, move to the cathode side, react and get into the flow-field on the cathode side again. The processes of species moving in and out of the flow-fields, along with the phenomena of species being dissolved into and released from the membrane phase, would affect the flow-fields on both the anode and cathode sides.

These phenomena have been considered in many existing PEM fuel cell models in the open literature [2,3,5,6,10,14]. However, deficiencies remain in these studies. First, models in the references [2,3,5,6,14] were based on the single-domain approach, and numerical approximations were made in handling water transport through the MEA. In the work of Dutta et al. [2], the MEA region was completely neglected from the computational domain while in the work of Siegel et al. [3], a water dissolution rate in the form of the convective mass transfer was used, but no formulation was introduced to calculate the dissolution coefficient. In the work of Wang and Wang [14], a fictitious water concentration treatment [12] was applied in MEA. As analyzed in [11,13], the fictitious water concentration treatment is theoretically valid in the catalyst layers but it lacks physical basis inside the membrane. It is not clear how water transport through the MEA was handled in [5,6]. The studies of Sivertsen and Djilali [10] were based on a multi-domain method with a fully-humidified membrane. Second, in the work of Hu et al. [5] and Wang and Wang [14], the conservation equations of species molar concentrations, instead of mass or molar fractions, have been solved. In reference [14], care was taken to ensure the consistency of the mass and species conservation equations.

Given all these weaknesses and uncertainties in the existing studies, the mixed-domain PEM fuel cell model [11] has been further extended to fully integrate the various transport phenomena. The formulation is based on fundamental transport and thermodynamic theories with assumptions properly justified and clearly stated. This three-dimensional mixed-domain PEM fuel cell model is then applied to investigate the effects of the fully-coupled transport phenomena on the cell performance, current distribution, and net water transfer across the membrane.

2. Theoretical formulation

The conservation equations of mass, momentum, species concentrations, proton and electron transport, and energy are derived in the following forms

Mass:

$$\nabla(\rho\vec{u}) = S_m \tag{1}$$

Momentum:

$$\frac{1}{\varepsilon^2}\nabla(\rho\vec{u}\vec{u}) = -\nabla p + \nabla\tau + S_{\mathrm{u}} \tag{2}$$

Species:

$$\nabla(\rho\vec{u}Y_i) = \nabla(\rho D_i^{\mathrm{eff}}\nabla Y_i) + S_i \tag{3}$$

Proton transport:

$$\nabla(\kappa^{\mathrm{eff}}\nabla\phi_{\mathrm{e}}) + S_{\mathrm{e}} = 0 \tag{4}$$

Electron transport:

$$\nabla(\sigma^{\mathrm{eff}}\nabla\phi_{\mathrm{s}}) + S_{\mathrm{s}} = 0 \tag{5}$$

Energy:

$$\nabla(\rho C_{\mathrm{p}}\vec{u}T) = \nabla(k^{\mathrm{eff}}\nabla T) + S_{\mathrm{T}} \tag{6}$$

An ideal equation of state is further applied herein to correlate pressure, density, and temperature,

$$p = \rho RT \tag{7}$$

where the parameter, R, is the gas constant, which is related to the universal gas constant in the following form:

$$R = \frac{R_{\mathrm{u}}}{W_{\mathrm{m}}} \tag{8}$$

The molecular weight of a mixture, W_{m}, can be calculated as:

$$W_{\mathrm{m}} = \left(\sum_{i=1}^{N}\frac{Y_i}{W_i}\right)^{-1} \tag{9}$$

In the mass conservation equation, the source term, S_{m}, arises from the coupling of the flow-field and the species transport processes, and its exact form will be developed later in this section. The source terms in the momentum equations will also be discussed later in this section. In the species conservation equations, the mass fractions, Y_i, are solved as the dependent variables. Since the summation of all the species equations will lead directly to the mass conservation equation, we will only need to solve $N-1$ species equations, where the parameter, N, is the total number of the species. The source terms in these species equations in the catalyst layers are derived as follows:

(a) for species except water:

$$S_i = -\frac{a_i j W_i}{nF} \tag{10a}$$

(b) for water:

$$S_{\mathrm{w}} = -\nabla\left(\frac{n_{\mathrm{d}}\vec{i}_{\mathrm{e}}}{F}\right)W_{\mathrm{w}} - \frac{a_{\mathrm{w}} j W_{\mathrm{w}}}{nF} \tag{10b}$$

In Eq. (10b), the electro-osmotic drag coefficient can be expressed as:

$$n_{\mathrm{d}} = \begin{cases} 1.0 \quad \text{for} \quad \lambda \le 14 \\ \frac{1.5}{8}(\lambda - 14) + 1.0 \quad \text{otherwise} \end{cases} \tag{11}$$

The electro-osmotic drag term at the interfaces of the membrane and the two catalyst layers will be determined using the interfacial boundary conditions, as developed later in this section. In deriving these equations, the electrochemical reactions are formulated in the following general form:

$$\sum_i a_i M_i = ne^- \tag{12}$$

The transfer current density, j in Eqs. (10), can be calculated using the Butler–Volmer equation. Details are presented in references [16,17].

In this mixed-domain approach, the equation of the water mass fraction will be solved only in the gas channels, gas diffusion layers, and the catalyst layers on both the anode and the cathode sides. Inside the membrane, a conservation equation of the water content is established [11],

$$\nabla(D_\lambda\nabla\lambda) + S_\lambda = 0 \tag{13}$$

where the source term arising from the electro-osmotic drag can be expressed as:

$$S_\lambda = -\nabla\left(\frac{n_{\mathrm{d}}\vec{i}}{F}\right) \tag{14}$$

In Eq. (13), the convective effect inside the membrane has been neglected, and the water content diffusivity, D_λ, is given in [11].

A set of internal boundary conditions at the interfaces between the membrane and the catalyst layers on the anode and cathode sides is required to connect the water mass fraction and the water content equations. Based on thermodynamic phase equilibrium [18] and flux equality, the general forms of the interfacial boundary conditions are:

$$p^{\mathrm{m}} = p^{\mathrm{cl}} \tag{15a}$$

$$T^{\mathrm{m}} = T^{\mathrm{cl}} \tag{15b}$$

$$\mu_i^{\mathrm{m}} = \mu_i^{\mathrm{cl}} \tag{15c}$$

and,

$$\dot{m}^{\mathrm{m}} = \dot{m}^{\mathrm{cl}} \tag{16a}$$

$$\vec{q}_{\mathrm{e}}^{\,\mathrm{m}} = \vec{q}_{\mathrm{e}}^{\,\mathrm{cl}} \tag{16b}$$

$$\vec{q}_i^{\,\mathrm{m}} = \vec{q}_i^{\,\mathrm{cl}} \tag{16c}$$

The schematic of the interface and the related boundary conditions are shown in Fig. 1.

In Eqs. (15) and (16), the parameter i, is from 1 to $N-1$. Furthermore, we have:

$$\dot{m} = \sum_{i=1}^{N}\vec{q}_i \tag{17}$$

As described in [11], Eq. (15a) is required for solving water transport in the membrane once liquid water is involved, as suggested in Weber and Newman [19]. In the present pseudo single-phase PEM fuel cell model, this boundary condition is

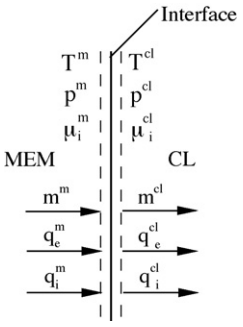

Fig. 1. Schematic of an interface and the related interfacial boundary conditions.

neglected. Since the single-domain method is used for solving the energy equation, Eqs. (15b) and (16b) will be closely approached but are not explicitly required. Eqs. (15c) and (16c) indicate that these interfacial boundary conditions are valid for all the species conservation equations. Since the concentrations of the other species, except water, inside the membrane are generally not required in PEM fuel cell modeling, the interfacial boundary conditions for these species equations can be neglected. The cross-over fluxes of these species through the membrane, if needed, can be estimated approximately. Therefore, these species conservation equations can still be solved in the single-domain framework without resort to the interfacial boundary conditions. These cross-over fluxes are neglected in the present study. After these justified simplifications, only two boundary conditions from Eqs. (15c) and (16c) for water are needed at the interfaces of the membrane and the catalyst layers for connecting the water content equation inside the membrane and the water mass fraction equation in the other regions. As presented in [11], these two boundary conditions can be further developed as:

$$\lambda = \begin{cases} 0.043 + 17.81a - 39.85a^2 + 36.0a^3 & 0 < a \le 1 \\ 14 + 1.4(a-1) & 1 < a \le 3 \end{cases} \tag{18a}$$

$$\vec{q}_{\mathrm{w}} = W_{\mathrm{w}} \left(-D_{\lambda} \nabla \lambda + \frac{n_{\mathrm{d}} \vec{i}}{F} \right) \Bigg|_{\mathrm{m}} = (-\rho D_{\mathrm{w}}^{\mathrm{cl,eff}} \nabla Y_{\mathrm{w}} + \dot{m} Y_{\mathrm{w}})|_{\mathrm{cl}} \tag{18b}$$

In Eq. (18b), water transport in the membrane phase inside the two catalyst layers has been considered using the fictitious water concentration treatment [11–13], and the effective water diffusivity in the catalyst layers is provided in [11].

After neglecting the interfacial fluxes of the other species except water, the mass flux across the interface in Eq. (17) becomes:

$$\dot{m} = \vec{q}_{\mathrm{w}} \tag{19}$$

This is the interfacial boundary condition for the mass conservation equation. Since in the present PEM fuel cell model, velocity inside the membrane is neglected as it is very small, this boundary condition is required only in the two catalyst layers. In order to maintain the single-domain approach for the mass conservation equation, this interfacial mass flux is converted into a source/sink term as:

$$S_{\mathrm{m},i} = \dot{m} \times \frac{\Delta A_i}{\Delta V_i} \tag{20}$$

where the parameters, ΔA_i and ΔV_i, are the interfacial area and volume of a cell in the catalyst layer neighboring the membrane.

Now the source/sink term in the mass conservation equation in the present pseudo single-phase PEM fuel cell model can be derived as:

$$S_{\mathrm{m}} = \sum_{i=1}^{N} S_i + S_{\mathrm{m},i} \tag{21}$$

Similar expressions are also provided in [14,15].

In fact, the mass flux and the electro-osmotic drag term would impose effects on the momentum equations as well, but the effects are extremely small, compared with the effect of the Darcy's term, and are thus neglected in the present PEM fuel cell model.

The exact forms of the source/sink terms in the momentum, proton and electron transport, and energy equations, and the relevant physicochemical and transport parameters could be found in references [16,17,20]. The anisotropic transport phenomena in PEM fuel cells could be handled using a simplified treatment introduced in [21].

The conservation equations in Eqs. (1)–(7) and (13), and the interfacial boundary conditions in Eqs. (18a) and (18b) constitute the present three-dimensional mixed-domain PEM fuel cell model with fully-coupled transport phenomena. The relevant source terms, physicochemical relationships, boundary conditions, and numerical treatments can either be found in this paper or follow the same procedures as in the single-domain approach, as detailed in references [16,17,20]. In this model, after fully justified simplifications, only one set of interfacial boundary conditions is required to connect the water content equation inside the membrane and the water mass fraction equation in the other regions. All the other conservation equations are still solved in the single-domain framework. This model is applicable to the nine regions in a PEM fuel cell, including the current-collecting plates, gas channels, gas diffusion layers, and catalyst layers on both the anode and cathode sides, and the membrane.

3. Result and discussion

This numerical model has been implemented into a general CFD package, Fluent, and it is then applied to investigate the effects of the coupled transport phenomena on the detailed PEM fuel cell performances. The PEM fuel cell studied is a single straight-channel cell with a thin membrane of 25 μm. Its geometry is illustrated in Fig. 2, and the related geometric and input parameters are presented in Tables 1 and 2, respectively. In the present configuration, the x-coordinate is in the through-membrane direction, y-coordinate the along-channel direction, z-coordinate the lateral direction. The cell is operated at a constant temperature of 80 °C, and its inlet stoichiometry numbers are two based on a reference current density of 1 A cm^{-2} on both

Table 1
Cell geometric parameters

Fuel cell geometry (mm)		
Cell length		100
Gas channel	Depth	1
	Width	1
Layer thickness	Diffusion	0.3
	Catalyst	0.01
	Membrane	0.025
Land width		0.5
Computational cell numbers		~320,000

Table 2
Input parameters

Anode volumetric exchange current density, aj_0 ($A\,m^{-3}$)	$1.0E+9$
Cathode volumetric exchange current density, aj_0 ($A\,m^{-3}$)	$1.0E+4$
Reference hydrogen concentration, C_{H_2} ($mol\,m^{-3}$)	40
Reference oxygen concentration, C_{O_2} ($mol\,m^{-3}$)	40
Anode transfer coefficients	$\alpha_a = \alpha_c = 1$
Cathode transfer coefficient	$\alpha_c = 1$
Faraday constant, F ($C\,mol^{-1}$)	96487
GDL porosity	0.6
Porosity of catalyst layer	0.12
Volume fraction of ionomer in catalyst layer	0.4
GDL permeability (m^2)	$1.0E-12$
Equivalent weight of ionomer ($kg\,mol^{-1}$)	1.1
Dry membrane density ($kg\,m^{-3}$)	1980
Electronic conductivity in current collector ($S\,m^{-1}$)	20000
Effective electronic conductivity in GDL ($S\,m^{-1}$)	5000
Operation temperature (°C)	80
Operation pressure (atm)	2
Anode stoichiometry	2
Cathode stoichiometry	2

the anode and cathode sides. Two different cases are designed for the present numerical study, as shown in Table 3. Since the cell operates at a constant temperature of 80 °C, both cases are in low-humidity operation conditions, consistent with the present pseudo single-phase calculations. In the present numerical calculations with fully-coupled transport phenomena, hydrogen and water are fed into the anode inlet while air and water into the cathode inlet. Therefore, only the conservation equation of the water mass fraction is solved on the anode side, while the conservation equations of water and oxygen mass fractions are solved on the cathode side. Numerical results from the prior mixed-domain model [11], which decouples the flow-field from the species transport processes, are also provided for comparisons. The computational grid used in the present numerical study is the same as in the previous work [16,22], which is generated based on careful grid-independence studies.

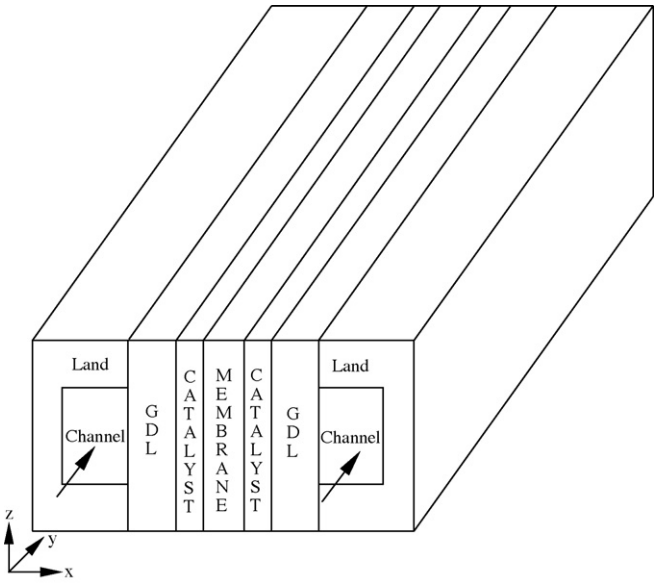

Fig. 2. Cell geometry.

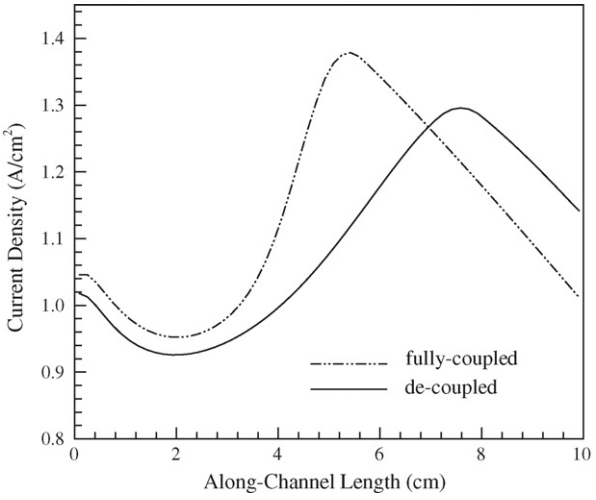

Fig. 3. Average current density variation along the channel direction in case 1.

Current density variations along the flow direction from case 1 are displayed in Fig. 3, in which the result from the present PEM fuel cell model with fully-coupled transport phenomena is compared with that from the decoupled method introduced in [11]. The two curves show the same trend, and the difference of the average current densities between them is less than 4% ($1.13\,A\,cm^{-2}$ for the fully-coupled model versus $1.09\,A\,cm^{-2}$ for the decoupled model), a result agreeing with that in [14]. However, the maximum currents from the two models occur at

Table 3
Inlet humidification temperature and relative humidity at cell temperature of 80 °C

Case number	Anode		Cathode	
	Humidification temperature (°C)	Relative humidity (%)	Humidification temperature (°C)	Relative humidity (%)
Case 1	80	100	20	5
Case 2	50	26	50	26

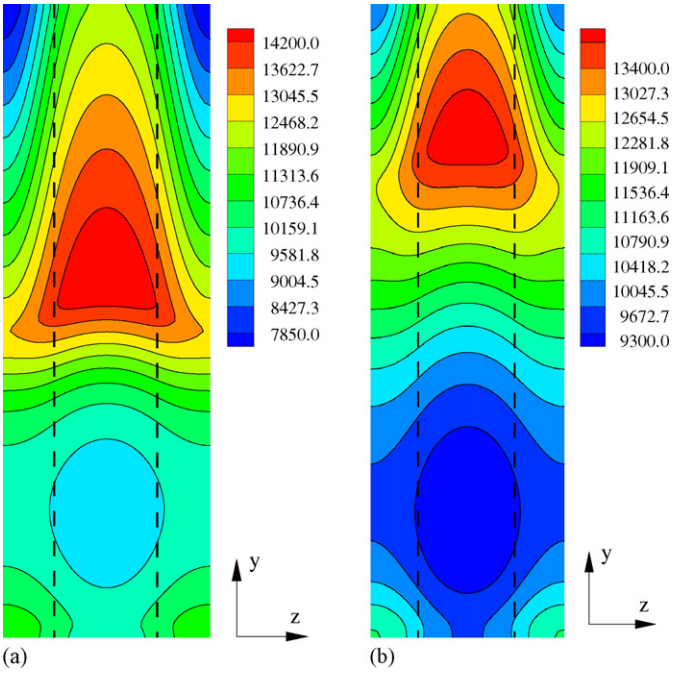

Fig. 4. Current density distribution in the mid-thickness plane of the cell inside the membrane in case 1: (a) from the fully-coupled model; and (b) from the decoupled model (unit: A m^{-2}).

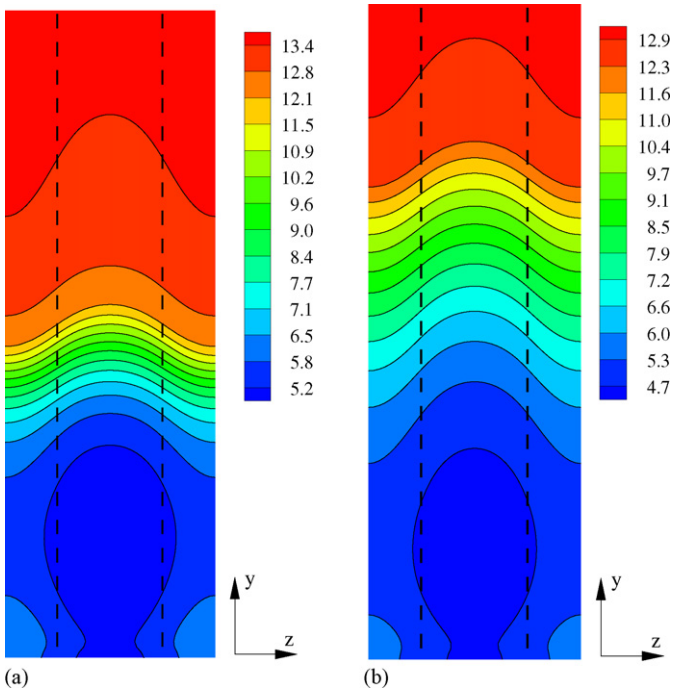

Fig. 5. Water content distribution in the mid-thickness plane of the cell inside the membrane in case 1: (a) from the fully-coupled model; and (b) from the decoupled model.

different locations; for example, the maximum current density in the fully-coupled model occurs in the middle of the cell length at $y = 5$ cm, but it shifts towards the exit in the decoupled model at $y = 8$ cm. The detailed current distributions from the two methods in the mid-thickness y–z plane inside the membrane are illustrated in Fig. 4, in which the difference of the results from the two models can be clearly seen.

Fig. 5 shows the water content distributions from the two models in the mid-thickness plane of the cell inside the membrane. The water content calculated from the fully-coupled model shows a drastic increase near the middle of the cell length, which contributes to the early increase of the current density, as shown in Fig. 4a, while the water content in the decoupled model varies smoothly in the along-channel direction.

Fig. 6 compares the variations of the net water transfer coefficient in the along-channel direction calculated from the two models. The net water transfer coefficient is defined as the ratio of the net water flux through the membrane to the proton flux,

$$\alpha = \frac{FN_{\mathrm{w}}}{I_{\mathrm{avg}}} \tag{22}$$

At the first half of the cell length, the net water transfer coefficients from the two models are in good agreement, but significant difference appears starting from the middle of the cell length. The net water transfer coefficient from the fully-coupled model drops into negative values around the middle of the cell length but rapidly rises into positive values. It remains negative in the decoupled model. The difference of the results between the two models reaches 0.18 at the exit of the cell. The average value of the net water transfer coefficient from the fully-coupled model is positive at around 0.18, consistent with the experimental analysis in [23] with a thin membrane and similar operation conditions.

A simple analysis indicates that the magnitude of the transverse velocity in the through-membrane direction is proportional to the net water transfer coefficient in the following form:

$$v \sim (W_{\mathrm{H_2}} + 2W_{\mathrm{W}}\alpha)I \tag{23}$$

Once the absolute value of the parameter, α, is slightly higher than 0.05, it would determine the direction of the transverse velocity, i.e. a positive value corresponding to positive velocity pointing from the anode to the cathode side and vice versa.

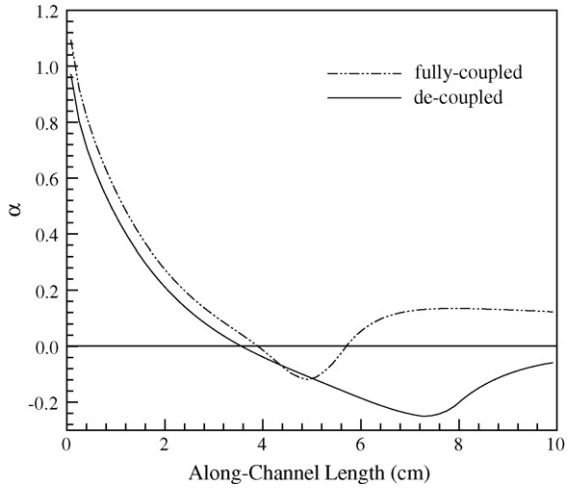

Fig. 6. Variation of the net water transfer coefficient along the channel direction in case 1.

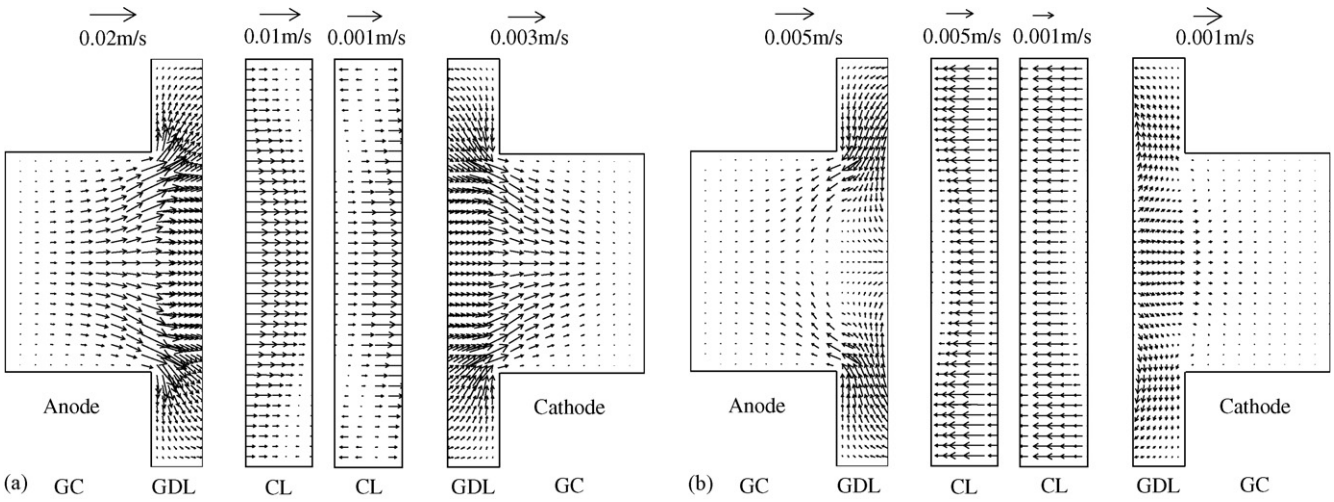

Fig. 7. Velocity distribution in the cross section perpendicular to the flow direction in case 1: (a) at the inlet region; and (b) in the middle of the cell.

Fig. 7 shows the velocity distributions in the x–z cross-section planes perpendicular to the inflow direction at two different locations. Fig. 7a shows velocity distributions in a cross-plane near the cell inlet region, where from Fig. 6, the net water transfer coefficient is positive, and therefore, the overall transverse velocity should point from the anode to the cathode side. Furthermore, the magnitude of the transverse velocity is larger under the gas channel than under the land, showing the dominant effect of the electro-osmosis. Fig. 7b shows velocity distributions in a cross-section in the middle of the cell length, where according to Fig. 6, the net water transfer coefficient is a negative value at around −0.12. Consistent with the above simple theoretical analysis, the overall transverse velocity is now negative pointing from the cathode to the anode side. In addition, the magnitude of the velocity is larger under the land than under the gas channel, indicating the dominant effect of water back diffusion.

In reference [14], a Peclet number has been used to indicate the relative strength of convection resulting from the transverse velocity to that of mass diffusion in GDL. The Pectet number is defined as:

$$Pe = \frac{u\delta_{\mathrm{GDL}}}{D} \tag{24}$$

Based on the velocity magnitude displayed in Fig. 7, the Peclet number at the two locations in Fig. 7 is at the order of 0.03, indicating that the convective term is far weaker than the diffusive one. However, although this Peclet number is very small, the fully-coupled transport processes still show significant effects on the current distribution and net water transfer coefficient, as shown in Figs. 3, 4 and 6. Therefore, it could be concluded that this Peclet number in GDL is not a crucial parameter to gauge the significance of the fully-coupled transport phenomena on PEM fuel cell operations. In fact, as will be discussed in the next sections, it is the intricate interactions of the mass transfer across the membrane, density and velocity variations, and species concentrations on both sides of the cell that produce the drastic effects on current distribution and net water transfer coefficient in the fully-coupled PEM fuel cell model.

Fig. 8 presents the average velocity and density variations along the flow direction in the anode and cathode gas channels scaled by their inlet values, respectively. On the anode side, instead of the assumed constant density and ensuing constant velocity along the gas channel from the flow-field calculation in the decoupled model, the density initially decreases, then increases, and finally stabilizes towards its inlet value. The velocity steadily decreases around 60% from its inlet value. Overall, the anode side loses around 60% of its inflow mass through hydrogen consumption and water transfer across the membrane. In the cathode gas channel, instead of the constant density and velocity obtained in the decoupled model, the density gradually decreases around 10% from the inlet to the outlet region while velocity increases more than 20%. On the cathode side, although mass is gained, density still decreases slightly. The reason is that it loses oxygen with higher density while it gains water with comparatively lower density. Overall, variations of the density and velocity in the cathode gas channel are small owing to the existence of a large amount of the inert gaseous

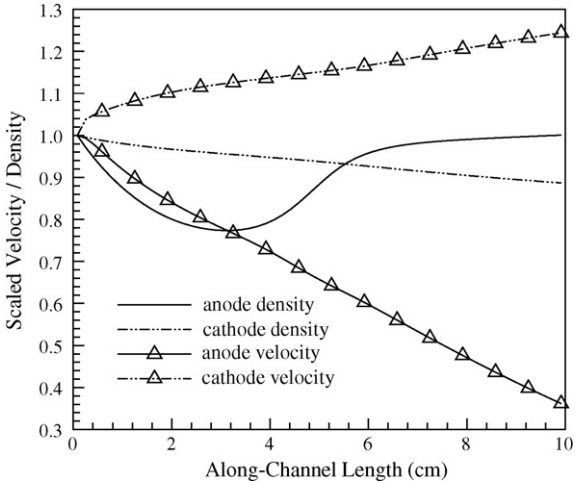

Fig. 8. Scaled average density and velocity variations in the gas channels on both sides of the cell in case 1.

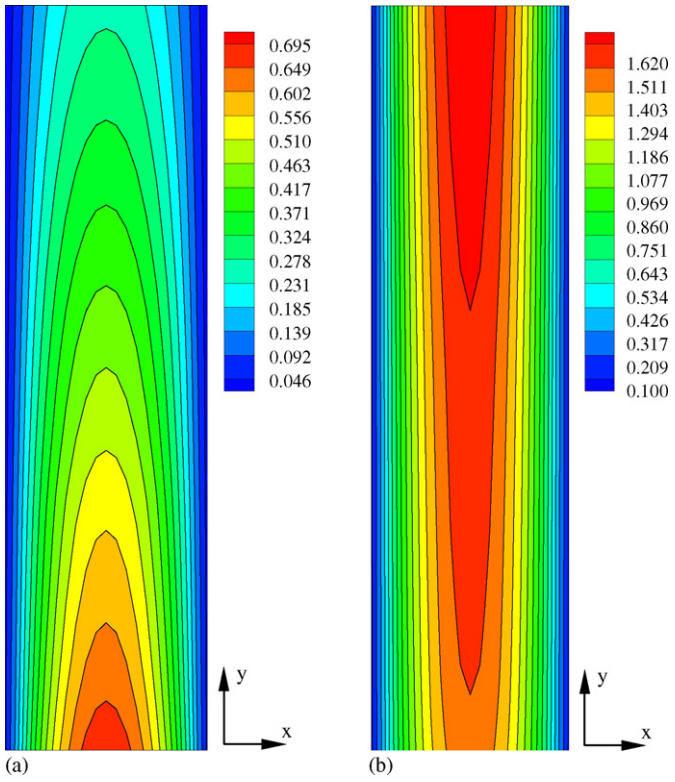

Fig. 9. Velocity distribution in the gas channel in case 1: (a) on the anode side; and (b) on the cathode side (unit: $m\,s^{-1}$).

nitrogen. Detailed velocity distributions in the gas channels on both sides are further displayed in Fig. 9.

Variations of the average molar concentrations of hydrogen and water in the anode gas channel and oxygen and water in the cathode gas channel along the flow direction are presented in Fig. 10, in which the hydrogen and oxygen concentrations are scaled by their respective inlet values while the water concentrations on both sides are scaled by their respective outlet values. The molar concentration of hydrogen on the anode side initially increases slightly and then stabilizes towards its inlet value. Overall, the hydrogen concentration calculated in the fully-coupled model maintains high values along the gas channel, consistent with the experimental results in [23]. This is in sharp contrast with the result in the decoupled model, which shows steady decrease of the hydrogen concentration with the electrochemical consumption and is thus inconsistent with the experimental results [23]. The water concentration in the anode gas channel varies in the opposite direction of the hydrogen concentration; it initially decreases resulting from water loss dictated by the electro-osmotic drag and then increases caused partly by the water back diffusion and partly by the decreasing velocity. Towards the anode exit, water concentration increases slightly, although net water is lost to the cathode side in this region, as shown in Fig. 6. This phenomenon and the high hydrogen concentration values throughout the cell can both be attributed to the significant velocity decrease. Therefore, in the fully-coupled PEM fuel cell model, there exist intricate interactions between the mass transfer across the membrane, density and species concentration variations, and velocity changes, which significantly affect the detailed fuel cell performances.

In Fig. 10, the oxygen concentration decreases almost linearly from the inlet to the outlet while water concentration increases significantly. Because the velocity and density variations on the cathode side are relatively small, as shown in Fig. 8, these species concentration variations could be easily correlated, as has been demonstrated in [23].

Fig. 11 compares the current density variations calculated from the fully-coupled and decoupled models in case 2. The two curves show the same increasing trend, and the difference between the average current densities is less than 4%. However, the maximum local difference at the exit region is very large, reaching 14%. The variations of the net water transfer coefficient from the two models are shown in Fig. 12. The values obtained from the present PEM fuel cell model with fully-coupled transport phenomena are always higher than those obtained from the decoupled model, and the gap becomes larger towards the exit region. At the exit, the gap reaches 0.06, showing more than 26% relative difference.

Variations of the scaled average hydrogen and water concentrations in the anode gas channel and oxygen and water

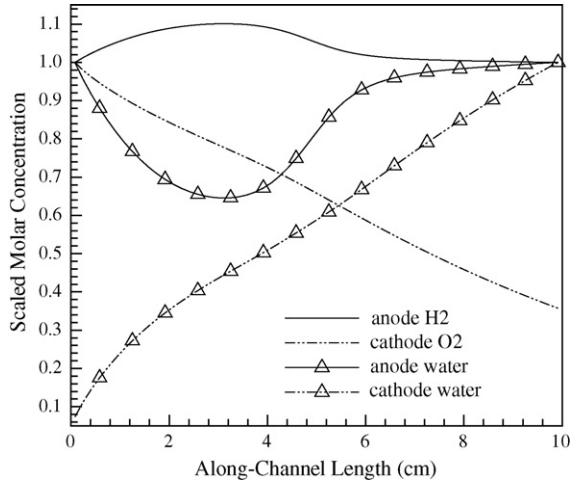

Fig. 10. Scaled average molar concentration variations in the gas channels on both sides of the cell in case 1.

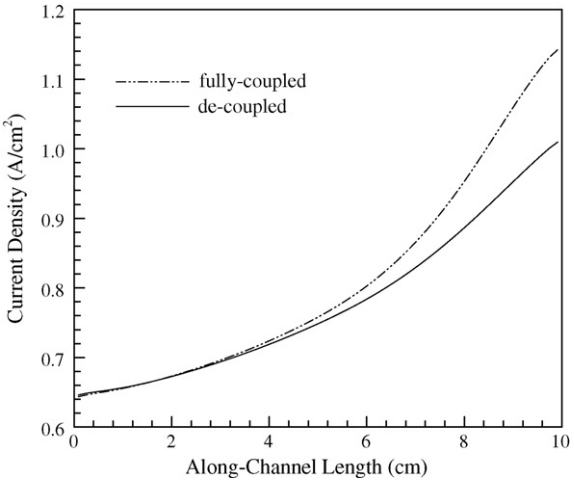

Fig. 11. Average current density variation along the channel direction in case 2.

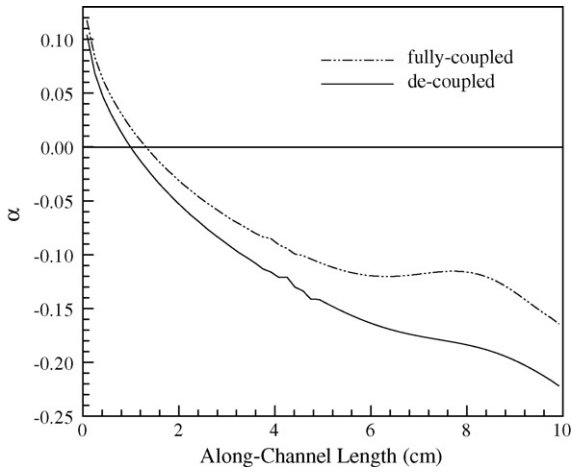

Fig. 12. Variation of the net water transfer coefficient along the channel direction in case 2.

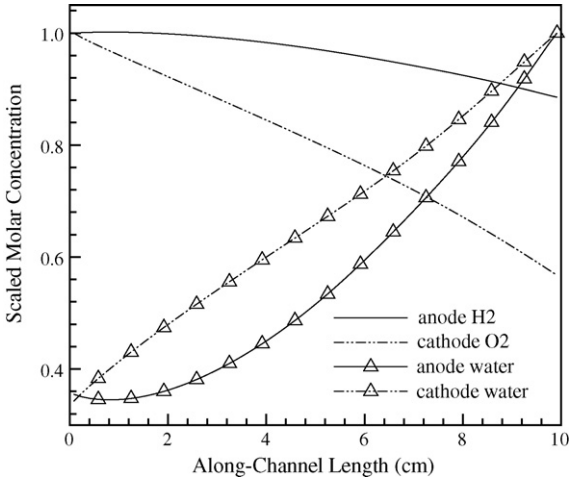

Fig. 13. Scaled average molar concentration variations in the gas channels on both sides of the cell in case 2.

concentrations in the cathode gas channel in case 2 are presented in Fig. 13. The hydrogen concentration on the anode side decreases slightly, but as in case 1, it maintains very high value throughout the entire cell.

4. Conclusion

In this paper, a previously developed three-dimensional mixed-domain PEM fuel cell model has been further extended to fully integrate the various transport phenomena. In this model, after fully justified simplifications, only one set of interfacial boundary conditions is required to connect the water content equation inside the membrane and the water mass fraction equation in the other regions. All the other conservation equations are still solved in the single-domain framework. This numerical model is applicable to the nine regions in a PEM fuel cell, including the current-collecting plates, gas channels, gas diffusion layers, and catalyst layers on both the anode and cathode sides, and the membrane.

Although the fully-coupled transport phenomena produce only minor effects on the overall PEM fuel cell performance, i.e. average current density, they make significant effects on current distribution, net water transfer coefficient, velocity and density variations, and species distributions in a PEM fuel cell. Therefore, for accurate PEM fuel cell modeling, the fully-coupled transport phenomena could not be neglected.

Numerical results indicate that the Peclet number defined in GDL, measuring the relative strength of convection to mass diffusion processes in the region, is not a crucial parameter to gauge the effects of the fully-coupled transport phenomena on the PEM fuel cell operations. In fact, there exist intricate interactions of the mass transfer across the membrane, electrochemical kinetics, density and velocity variations, and species distributions, which play a dictating role in determining the detailed cell performances.

References

[1] S. Um, C.Y. Wang, K.S. Chen, J. Electrochem. Soc. 147 (2000) 4485.
[2] S. Dutta, S. Shimpalee, J.W. Van Zee, Int. J. Heat Mass Transfer 44 (2001) 2029.
[3] N.P. Siegel, M.W. Ellis, D.J. Nelson, M.R. von Spakovsky, J. Power Sources 115 (2003) 81.
[4] S. Mazumder, J.V. Cole, J. Electrochem. Soc. 150 (2003) A1503.
[5] G. Hu, J. Fan, S. Chen, Y. Liu, K. Cen, J. Power Sources 136 (2004) 1.
[6] W.Q. Tao, C.H. Min, X.L. Liu, Y.L. He, B.H. Yin, W. Jiang, J. Power Sources 160 (2006) 359.
[7] V. Gurau, H. Liu, S. Kakac, AICHE J. 44 (1998) 2410.
[8] T. Berning, D.M. Lu, N. Djilali, J. Power Sources 106 (2002) 284.
[9] M. Hu, A. Gu, M. Wang, X. Zhu, L. Yu, Energy Convers. Manage. 45 (2004) 1861.
[10] B.R. Sivertsen, N. Djilali, J. Power Sources 141 (2005) 65.
[11] H. Meng, J. Power Sources 162 (2006) 426.
[12] S. Um, C.Y. Wang, J. Power Sources 156 (2006) 211.
[13] A.A. Kulikovsky, J. Electrochem. Soc. 150 (2003) A1432.
[14] Y. Wang, C.Y. Wang, J. Electrochem. Soc. 152 (2005) A445.
[15] C.Y. Wang, Chem. Rev. 104 (2004) 4727.
[16] H. Meng, C.Y. Wang, J. Electrochem. Soc. 151 (2004) A358.
[17] H. Meng, C.Y. Wang, Chem. Eng. Sci. 59 (2004) 3331.
[18] H.B. Callen, Thermodynamics and an Introduction to Thermostatistics, Second ed., John Wiley & Sons, 1985.
[19] A.Z. Weber, J. Newman, J. Electrochem. Soc. 150 (2003) A1008.
[20] H. Ju, H. Meng, C.Y. Wang, Int. J. Heat Mass Transfer 48 (2005) 1303.
[21] H. Meng, J. Power Sources 161 (2006) 466.
[22] H. Meng, C.Y. Wang, Fuel Cells 5 (2005) 455.
[23] X.G. Yang, N. Burke, C.Y. Wang, K. Tajiri, K. Shinohara, J. Electrochem. Soc. 152 (2005) A759.